Recombination between co-infecting herpesviruses occurs where replication compartments coalesce

Enosh Tomer[a], Efrat M. Cohen[a], Nir Drayman[b], Amichay Afriaat[a], Matthew D. Weitzman[c,d], Assaf Zaritsky[e,f,g] and Oren Kobiler[a]*

[a]Department of Clinical Microbiology and Immunology, Sackler School of Medicine, Tel Aviv University, Tel Aviv, Israel

[b]Institute for Genomics and Systems Biology and Institute for Molecular Engineering, University of Chicago, Chicago, IL, USA

[c]Department of Pathology and Laboratory Medicine, Perelman School of Medicine, University of Pennsylvania, Philadelphia, PA, USA

[d]Division of Protective Immunity, Children's Hospital of Philadelphia, Philadelphia, PA, USA

[e]Lyda Hill Department of Bioinformatics, UT Southwestern Medical Center, Dallas, TX, USA

[f]Department of Cell Biology, UT Southwestern Medical Center, Dallas, TX, USA

[g]Department of Molecular Cell Biology, Weizmann Institute of Science, Rehovot, Israel

Running title:

HSV-1 Recombination at colaescing replication compartments

* Corresponding author: Oren Kobiler, okobiler@post.tau.ac.il

Abstract

Recombination between co-infecting herpesvirus DNA genomes is an important process affecting viral population diversity and evolution. Each herpes simplex virus type 1 (HSV-1) replication compartment (RC) derives from a single incoming genome and maintains a specific territory within the nucleus. This raises intriguing questions about where and when co-infecting viral genomes interact. To study the spatiotemporal requirements for inter-genomic recombination, we developed an assay with dual-color fluorescence *in situ* hybridization enabling detection of homologous recombination (HR) between different co-infecting HSV-1 pairs. Our results revealed that when viral RCs enlarge towards each other, there is detectable overlap of genomes from each virus. Infection with paired viruses that allow visualization of HR correlates with increased overlap of RCs. Taken together, these findings suggest that HR events take place during replication of HSV-1 DNA and are mainly confined to the periphery of RCs when they coalesce.

40 **Importance**

41 Homologous recombination is considered a major driving force of evolution since it
42 generates and spreads genetic diversity. In the case of HSV-1, a ubiquitous human
43 pathogen that causes significant morbidity and mortality, evidence of homologous
44 recombination can be found frequently, both *in vitro* and in clinical isolates. Here we
45 designed an experimental system to detect where and when recombination takes
46 place between viral genomes during infection. We found that recombination events
47 occur after viral DNA replication during the late stages of infection, and is prevalent at
48 the interface of expanding viral replication compartments. Overall, our results provide
49 spatial and temporal information regarding the process of HSV-1 replication and
50 recombination, and these observations have implications for understanding the
51 recombination restrictions of other DNA viruses and cellular DNA.

52

53

54 **Introduction**

55 Herpes simplex virus type 1 (HSV-1) is a large double strand DNA virus. Like all other
56 herpesviruses, viral gene expression, replication and capsid assembly all occur in the
57 host nucleus of infected cells. Viral genomes enter the nucleus through the nuclear
58 pore complex as naked DNA molecules (1), and these rapidly recruit several host and
59 viral proteins to the viral genomes (2-10). Expression of the immediate early and early
60 viral genes allows initiation of viral DNA replication (11). HSV-1 DNA replication
61 proceeds at distinct foci within the nucleus known as replication compartments (RCs)
62 (12, 13). The formation of the viral RCs was suggested to initiate from small pre-RCs
63 (14, 15). Live cell imaging of viral DNA binding proteins suggested that the pre-RCs
64 migrate toward nuclear speckles, sites of RNA processing, and come into contact with
65 other pre-RCs, where they seem to coalesce into large mature RCs (16). On the other
66 hand, direct visualization of the viral DNA suggested that each RC usually emerges
67 from a single incoming genome (17, 18). Our previous study with Pseudorabies virus
68 (PRV - a swine alphaherpesvirus) suggested that although viral replication
69 compartments are found in close proximity, they retain distinct territories for each
70 individual genome (18). Earlier experiments with HSV replicons also supported this
71 notion (17). A recent study showed that viral genomes entering the nucleus are
72 observed as condensed foci, and suggested that viral expression and DNA replication
73 allow decondensation of these genomes and formation of RCs (19). Interestingly,
74 some genomes remain highly condensed at the edge of newly developing RCs (19).
75 Here, we visualised co-infecting HSV-1 genomes and confirmed that
76 alphaherpesviruses RCs initiate from single genomes.

77 Recombination is considered to be a major driving force in evolution of most organisms,
78 since it accelerates adaptation (20, 21). Viruses with double strand DNA genomes

need to adapt to the changing environment. Since the rate of mutation accumulation is lower for DNA viruses than that of viruses with RNA genomes (22, 23), it has been hypothesised that high rates of recombination can facilitate genetic adaptation (24). Indeed, homologous recombination (HR) among co-infecting HSV genomes is very frequently observed in both *in vitro* genetic assays (25-31) and in sequence analysis of clinical isolates (32-34).

Viral DNA recombination can be impacted by both viral and cellular proteins. Two viral proteins have been suggested to work as a complex to facilitate viral recombination and have been shown to catalyze strand exchange *in vitro*: the single strand binding protein ICP8 and an exonuclease UL12 (35). Single strand annealing was found to be a recombination mechanism upregulated during viral infection and thus is considered as the mechanism by which the viral recombinase induces recombination (36). While ICP8 is required for viral DNA replication, UL12 is not essential for DNA replication *per se*, although it is required for formation of infectious viral genomes that can be packaged into capsids (37). Recombination of HSV-1 genomes can be enhanced by DNA double stand breaks (DSB) (31, 38) and components of cellular DSB repair pathways are recruited to sites of viral DNA replication (4, 6, 8, 39, 40). Host proteins that are known to be involved in host HR, were found to support either viral DNA replication or production of infective viral progeny (4, 39, 41-43). These findings suggest that viral recombination and replication are processes that are closely related (44). While knowledge regarding the molecular aspects of HR has been accumulating over the last few years, little is known regarding spatiotemporal constraints on inter-genomic recombination.

The compartmentalization of co-infecting genomes at different RCs raises the question of where and when recombination takes place during the course of infection. To tackle

104 this question, we utilized a fluorescence *in situ* hybridization (FISH) based assay to
105 differentiate between *de-novo* synthesized variants of viral genomes. Our results
106 suggest that multiple recombination events occur at later stages of infection following
107 DNA replication and that recombination takes place at the interface between mature
108 RCs. We also found strong evidence of correlation between the number of RCs and
109 nuclear size, suggesting a possible spatial restriction on the number of viral genomes
110 that initiate replication.

111 **Results**

112 **A FISH based assay designed to detect recombination events between co-**
113 **infecting viruses.** Recombination among co-infecting HSV-1 strains is a frequent
114 event that can be detected by the progeny viruses released from infected cells (27-29,
115 31). To study the spatiotemporal constraints of these recombination events we
116 developed a FISH based experimental assay that enables visualization of two different
117 viral genomes within a co-infected nucleus. For this assay, we constructed a series of
118 viral isolates, isogenic to each other except for two unique tag sequences (YPET or
119 mCherry, yellow and red fluorescent proteins encoding genes, respectively) inserted
120 into various loci throughout the viral genome (Figure 1A and Table 1). We designed
121 two sets of fluorescent probes, one set for each tag sequence (Figure 1B). Each probe
122 set was conjugated to a distinct fluorophore (Cy3 or Cy5) to enable visual identification
123 of the genomes containing each tag sequence. We hypothesize that using different
124 mixtures of the viruses should lead to distinct patterns within the infected nucleus
125 (Figure 1C). As was shown previously for PRV (18), we expect that co-infection with
126 two HSV-1 viruses containing tag sequences at the same genomic locus cannot result
127 in a new recombinant genome containing both tags. Thus, each RC will react to a
128 single fluorophore, including at the contacting edges of proximate RCs (Figure 1C

129 example I). Infection with a viral recombinant containing two tag sequences within one
130 genome is expected to result in RCs stained with both fluorophores (dually-labelled
131 RCs) (Figure 1C example IV). Infection with two viral recombinants containing tag
132 sequences at different genomic loci could result in progeny genomes that either
133 contain both tag sequences on a single genome or contain neither tag sequence. One
134 of two types of spatial patterns could be expected to dominate under these conditions.
135 Dually-labelled RCs (fully covered by both probe sets) imply that recombination takes
136 place early during infection before the viral DNA replicates and RCs mature. In this
137 situation, the reciprocal recombinant genome would contain no tag sequences and will
138 generate RCs that are not detected since they are not covered by any of the probes
139 (Figure 1C example II). Alternatively, partially overlapping RCs that fuse to each other
140 at their periphery, suggest that recombination occurs later during the infection cycle
141 following viral DNA replication (Figure 1C example III). Therefore, this FISH assay is
142 designed to detect viral recombination events, with visual readouts for when and
143 where it takes place.

144 **Patterns of RC interactions dependent on HR.** To identify recombination events,
145 we co-infected Vero cells with different pairs of viruses listed in Table 1, as detailed
146 below. All infections were carried out at MOI 20, to increase the likelihood of
147 interactions between incoming viral genomes (27). Cells were either infected with one
148 virus that contained both mCherry and YPET tag sequences (OK31) or were co-
149 infected with two viruses, each carrying a different tag sequence (OK35 together with
150 either OK25, OK32 or OK26). First, we collected the progeny viruses released from
151 the infected cells at 24 hours post infection (HPI) and plated for single plaques. When
152 the fluorescent protein genes are at different sites in the viral genomes, we found that
153 co-infections can result in dual color (yellow) plaques under our infection conditions

154 (Figure 1D), suggesting that progeny viruses can be the outcome of HR events (27).
155 To visualize HR events at the single cell level, cells were co-infected and fixed at 6HPI
156 for hybridization with the appropriate fluorescent probes. Using confocal fluorescent
157 microscopy, we imaged the viral RCs and identified four distinct patterns of
158 interactions between the RCs (Figure 2A-D). The first interaction type is of two RCs
159 that come into close contact but without evidence of mixing between the two RCs i.e.
160 no visible co-localized pixels and no intersection between RCs margins (Figure 2A).
161 These interactions were mostly observed when the tag sequences were at the same
162 genomic locus (OK25 and OK35, Figure 2E). The second interaction type is of two
163 RCs that come into close contact and clearly mix, as defined by the presence of dual
164 color pixels at the site of contact or blurring of the contacting edges (Figure 2B). This
165 was the most common interaction observed in all co-infections, particularly when the
166 two tag sequences were located further from each other on the viral genome (OK26
167 and OK35, Figure 2E). In the third interaction type, one RC seems to be fully
168 overlapped with part of a second RC that is usually much larger (Figure 2C). This
169 interaction was most prevalent with co-infection of the OK32 and OK35 viruses (Figure
170 2E). The last interaction is a dual color RC, in which the entire area of the RC contains
171 both fluorophores (Figure 2D). The relative frequencies of these events can be
172 quantitated during single or dual infections (Figure 2E). As expected, the overlapping
173 pattern accounted for almost 90% of RCs in cells with single infection of virus carrying
174 both tag sequences (OK31), and was rarely detected during co-infections. We deduce
175 that our assay can be used to readout recombination, since detectable HR events
176 change the overall distribution of the interactions among the RCs. In all co-infection
177 assays, partial overlap at the point of contact are more frequent, compared to entirely
178 overlapping RCs. The rare occurrence of entirely overlapping RCs compared to the

179 expected high frequency of HR during HSV-1 co-infection (31) suggest that these RCs
180 are unlikely to reflect most of the HR events. We therefore suggest that inter-genomic
181 HR occur at points of physical interaction between co-infecting genomes, after viral
182 DNA replication has initiated.

183 We have previously shown that in U2OS cells, on average more HSV-1 genomes
184 initiate expression per cell compared to infections of Vero cells (45). To test if the
185 number of initiating genomes has an effect on the interactions between RCs, we
186 repeated the FISH based experiments with infections of U2OS cells. We observed all
187 four patterns of RCs interactions that we defined for infections of Vero cells (Figure 3).
188 However, in U2OS cells, identifying more than one pattern in a single cell was more
189 common than in Vero cells (Figure 3A and 3B), probably due to the higher number of
190 RCs observed per cell in this cell type (see below, Figure 5A). The distribution of
191 patterns observed for the different infections in U2OS cells (Figure 3D) was similar to
192 the distribution detected in Vero cells (Figure 2E).

193 **Overlap between RCs is enhanced by HR.** Identifying patterns does not estimate
194 the relative proportion of overlapping areas between RCs. Therefore, we developed a
195 quantitative evaluation of the RC overlapping areas in each cell. We found that
196 common pixel based co-localization methods do not provide an accurate estimate of
197 the degree of overlap between HSV-1 RCs, probably due to the relaxed form of the
198 replicating viral DNA (19). Similar to our results with infection of virus carrying the two
199 tag sequences (OK31), two probes corresponding to adjacent loci on HSV-1 genomes
200 showed limited co-localization at the pixel level (46). We applied a semi-automated
201 object based method to quantify the degree of overlap for RCs in cells infected with
202 viruses that have two distinct genomes (see Methods). For each cell nucleus, we
203 independently segmented the RCs in each channel. The relative overlapping area was

204 calculated as the ratio between the overall area of the overlap and the total overall
205 area occupied by viral DNA (total area of all RCs minus the total overlap area). The
206 images analysed were collected from three infections carried out on different days
207 from separate viral stocks. Over 200 cells from each cell type were analysed for each
208 co-infection. The dual-tagged virus (OK31) had such a distinct and reproducible
209 pattern, that only 120 Vero and 99 U2OS cells were analysed. We calculated the
210 percentage of cells in which no overlap was identified (Figure 4A-B). Some of these
211 cells resulted from RCs that were spatially distant, while others had interactions that
212 did not result in any mixing between coalescing RCs. For both cell types, when the
213 sequences are at the same site on the viral genome and therefore do not allow
214 visualization of HR between RCs (OK25 and OK35, Blue columns), only about 25% of
215 the cells had no measured colocalization. In U2OS cells, the possibility of HR reduced
216 the number of cells without colocalization to ~8.5% (OK35 and either OK32 or OK26,
217 yellow and orange columns respectively). In Vero cells, the possible visualization of
218 HR had much lower effect, probably due to higher probability for no interactions
219 between the RCs. These results suggest that when HR is possible to detect between
220 co-infecting viruses, interactions between RCs are observed more frequently.

221 We analysed all the cells in which co-localization was observed. For both cell types
222 we found a significant increase in the relative overlapping area for each nucleus for
223 cells infected by viruses with tags in different loci (Figure 4C-D). The resolution of our
224 FISH assay was not sufficient to detect significant differences between the two co-
225 infections with viruses that have tags in different loci. To test that cellular parameters
226 did not bias our measurements, we compared the relative overlapping area to the
227 nuclear area (Figure 4E-F) or to the number of RCs per nucleus (not shown). We found
228 no evidence of correlation between these two parameters to the relative overlapping

229 area in all infection conditions (Pearson correlation bellow 0.3 for each of the
230 infections). We conclude that the observed significant increase in overlapping area
231 indicates the readout of HR events. We speculate that the relative high background
232 levels of overlapping areas (~20%) are due in part to noise of the assay and to non-
233 HR events during viral replication.

234 **The number of RCs correlates with nuclear size.** The ability to distinguish between
235 coalescing RCs in our assay provides an opportunity to quantitate the number of
236 mature RCs within individual cells. We note that the OK31 infection was omitted from
237 the calculation in this section due to our inability to distinguish between coalescing
238 RCs in this infection. We therefore tested the association of the number of RCs to
239 other parameters of infection. First, we observed that in U2OS cells more RCs were
240 detected per individual nucleus. We detected an average of ~5.1 RCs per nucleus in
241 U2OS cells compared to ~3.7 RCs per nucleus in Vero cells (1.375 fold increase,
242 Figure 5A). Interestingly, a similar fold increase of ~1.38 was identified in nuclear area
243 (Figure 5B). This led us to speculate the existence of a correlation between nuclear
244 area and the number of RCs per nucleus. Indeed, the number of RCs correlates to the
245 nuclear area for individual cells of both cell types (Pearson correlation: $R > 0.538$ for
246 all infections, $p < 0.0001$ for all infections, Figure 5C-D). We hypothesize that the
247 increase in the number of RCs per nucleus will result in a total of more viral DNA (RCs
248 area) in larger nuclei. As expected, the nuclear area correlates to the total area of the
249 RCs per nucleus (Pearson correlation: $R = 0.530$ for OK32 and OK35 co-infection on
250 Vero and $R > 0.625$ for all other infections, $p < 0.0001$ for all infections, Figure 5E-F).
251 We speculated that the increase in total RCs area could also result from the possibility
252 that RCs may expand faster to a larger size in larger nuclei. We therefore compared
253 the mean RC area (per cell) to the nuclear area (Figure 5G-H). We found much weaker

254 correlation between these parameters (Pearson correlation: < 0.5 for U20S cells and
255 < 0.3 for Vero cells in each of the infections). These results suggest that the increase
256 in RC area in larger nuclei results from higher numbers of RCs rather than increased
257 RC size. Taken together, our results suggest that nuclear size is a limiting factor for
258 the number of incoming genomes that are able to initiate replication.

259 **Triple-color FISH indicates that inter-genomic recombination occurs at edge of**
260 **coalescing RCs.** We speculated that if there are RCs that originate from a single
261 recombinant genome and contain both tag sequences, there must be reciprocal
262 recombinant RCs that contain none of the tags and are undetectable in our FISH assay
263 (Figure 1C II). To determine whether these RCs exist, we designed an additional
264 probe conjugated to a third fluorophore corresponding to the genomic HSV a'
265 sequence, a repetitive sequence found in four copies within the HSV-1 genome (47),
266 This probe stains all HSV-1 viral DNA regardless of the tag sequence inserted. Both
267 Vero and U2OS cells were co-infected with two isolates containing tags at different
268 genomic loci, fixed and hybridized to all three probes as previously described. We
269 inspected over 600 RCs from each cell type and found that 99.6% stained by the HSV
270 non-specific probes reacted to either of the two specific probe sets (example in Figure
271 6). The existence of at least one tag sequence for all RCs suggests that RCs are not
272 generated from recombinant genomes. This result further supports the hypothesis that
273 recombination occurs at the edge of mature coalescing RCs at the later stages of
274 infection and is coupled with replication. Similarly, all areas at the interaction between
275 the mature RCs respond to both the specific probe sets in contrast to our prediction in
276 Figure 1C III. This suggests that areas containing recombinant DNA do not arise from
277 a single recombination event but rather from multiple events along the contact front of

278 replicating RCs. In other words, the overlapping areas contain a mixture of genomes
279 with one tag, both or none of them.

280 Discussion

281 Recombination among co-infecting herpesviruses is fundamentally important for
282 understanding viral evolution and pathogenesis (24). It is also important to consider
283 recombination when developing vectors for vaccination and oncolytic viral therapy,
284 since evidence for recombination between a vaccine strain and a wild type strain has
285 already been found in herpesviruses (48). Here, we developed a unique experimental
286 system to identify the spatiotemporal constraints of inter-genomic recombination. Our
287 results corroborate the hypothesis that each RC initiates from a single incoming
288 genome. We showed that the possibility to visualize HR increases the overlapping
289 areas between RCs, although the experimental system also detects overlapping
290 signals unrelated to HR. We found that most viral recombination events occur at the
291 edges of developing RCs where they coalesce with others. Finally, we suggest that
292 areas in which overlapping RCs are detected, result from multiple independent
293 recombination events.

294 We have infected cells with different combination of viral isolates: OK35 & OK25 where
295 tags are inserted into the same genomic locus, OK35 & OK32 containing tags on
296 separate genomic loci spaced approximately 72 Kbp apart, OK35 & OK26 spaced
297 approximately 105 Kbp apart and OK31 containing two tag sequences on a single viral
298 genome. In our analysis, we have not detected any significant differences between the
299 two combinations of the separate genomic loci (i.e. OK35 & OK32 and OK35 & OK26),
300 in agreement with the hypothesis that recombination events occur between replicating
301 genomes in either concatemeric or circular state (26).

302 We observed four recognizable patterns of interactions between adjacent RCs: i. no
303 mixing, ii. partial mixing, iii. one within another and iv. complete overlap (Figure 2 and
304 3). From our previous results with PRV (18), we expected that the no mixing of RCs
305 would be the dominant interaction following co-infection with two viruses carrying the
306 tag sequences at the same location in the viral genomes (OK25 and OK35). We found
307 that this readout is most commonly observed in this co-infection, although to our
308 surprise the majority of RCs (~66%) showed some degree of mixing. Comparison with
309 the images obtained in the Kobiler *et al.* paper suggested that there is no major
310 difference between the images from the two alphaherpesviruses co-infection, although
311 robust quantitative analysis of PRV images was not carried out.

312 The partial mixing of RCs was the most common interaction observed among the
313 different co-infection conditions tested (Figure 2E). This is in part due to the
314 categorization of all partial mixing interactions into one single pattern, regardless of
315 the proportion of mixing. To overcome this problem, we developed an image analysis
316 code that calculates the relative area of mixing. We found a significant increase in the
317 relative area of mixing when co-infections were carried out with viruses in which HR
318 can result in the mixing of the colors. These measurements were significant both at
319 the single cell level (Figure 4C and D) and at the single RC level, indicating that a
320 significant proportion of the mixing we observe is due to HR. On the other hand, even
321 when HR cannot result in signal mixing (i.e. OK25 and OK35 co-infection), we
322 observed RCs and cells in which high proportion of mixing occurred (Figure 4E and
323 F). Similar findings were found in the PRV co-infection assays (18). These results
324 suggest that some color mixing can occur without recombining both tag sequences
325 into the same genome, or that there are high levels of non-HR that take place during
326 viral replication. We note that non-HR events were observed previously both in HSV-

327 1 replication (49) and in other herpesviruses (50). These explanations are not mutually
328 exclusive, and probably both contribute to the mixing of colors observed without HR.

329 The interaction in which one RC is fully mixed into a larger RC (Figure 2C) can be
330 explained by different mechanisms. First, it could originate from a small RC that
331 coalesces with a larger one. Second, the smaller RC could interact with two larger
332 RCs from both sides of the small RC that eventually unite to a single larger RC. A third
333 mechanism could involve the recently observed condensed viral genomes at the edge
334 of RCs (19). Sekine *et al.* showed that at 3HPI several incoming genomes remain
335 condensed at the periphery of an enlarging RC. These condensed genomes might be
336 silent throughout the lytic infection or may serve as templates for recombination at
337 later time points (which will result in our observed third interaction). Further
338 experiments are required to distinguish between these different possibilities.

339 Our experimental system provides the opportunity to calculate accurately the number
340 of functional RCs within a nucleus, since the separation by color increases our ability
341 to differentiate between coalesced RCs. We were able to detect an increase in the
342 average number of RCs detected in U2OS nuclei compared to Vero nuclei. This
343 corroborates our previous finding that in U2OS cells on average a higher number of
344 incoming viral genomes per cell initiate expression and replication compared to Vero
345 cells (45). These observations also further support the emerging view that individual
346 RCs initiate from single incoming genomes (18).

347 We previously demonstrated that the number of HSV-1 genomes replicating per cell
348 can influence the outcome of infection (51) and that host conditions prior to infection
349 can also affect the outcome of infection at the single cell level (51, 52). Here, we define
350 correlations between the nuclear area and the number of detectible RCs, similar to the

351 correlation between cell size (as measured by flow cytometry) and the number of
352 replicating genomes (51). Since our images represent snapshot during the infection
353 process, we cannot distinguish between the possibilities that larger nuclei allow a
354 larger number of incoming viral genomes to initiate replication or that the nuclei in
355 which more genomes initiated replication, expand faster. The use of new methods to
356 visualise incoming genomes using click chemistry (19, 53) should be able to resolve
357 these two hypotheses. We note, that U2OS cells are known to have larger nuclei and
358 indeed have more RCs per cell than Vero cells, suggesting that the larger nuclei
359 support more incoming viral genomes. On the other hand, U2OS are known to be
360 missing parts of the intrinsic immunity (54-56) and therefore that could explain the
361 difference in number of genomes.

362 In conclusion, our results support a model in which incoming viral genomes establish
363 RCs at distinct sites in the nucleus. The vast majority of RCs initiate from a single
364 genome and only at later stages coalesce but maintain a detectable separation
365 between RCs. These areas of interactions between the expanding RCs are predicted
366 to be the site in which HR occurs in tight association with viral DNA replication. Our
367 results suggest that in these sites, recombination is a frequent event, although not all
368 areas of interactions between the RCs are supportive of close contact that can lead to
369 recombination. Further research will shed light on the differences between these types
370 of RC interactions.

371

372 **Materials and methods**

373 **Cell culture**

374 African green monkey kidney cells (Vero, ATCC CCL-81) and human female
375 osteosarcoma cells (U2OS cells ATCC HTB-96) were grown in Dulbecco's Modified
376 Eagle Medium (DMEM X1; Gibco), supplemented with 10% Fetal Bovine Serum (FBS;
377 Gibco) and 1% Penicillin (10,000 units/ml) and Streptomycin (10 mg/ml; Biological
378 Industries, Israel).

379 **Viruses**

380 All viral recombinants are derivatives of herpes simplex type 1 strain 17. Each viral
381 recombinant contains one or two tag sequences for specific staining by FISH. To
382 facilitate isolation, both tag sequences are expression constructs for fluorescent
383 proteins. The red fluorescent protein mCherry driven by the human cytomegalovirus
384 promoter (CMVp) and the yellow fluorescent protein YPET driven by the simian virus
385 40 promotor (SV40p). Tag sequences were inserted into the viral genome by
386 homologous recombination. Viral DNA was co-transfected along with a plasmid
387 containing the tag sequences flanked by sequence homologies to the viral site of
388 insertion (synthetically generated by GenScript, Piscataway, NJ, USA). Recombinant
389 viruses were isolated from the progeny by plating lysate from transfected Vero cells
390 and picking fluorescent plaques using an epi-fluorescent microscope. Viral stocks
391 were prepared by growing purified plaques for each recombinant virus on Vero cells.
392 The viral recombinants were validated by PCR. Viral titters were measured by plaque
393 assay. An additional viral recombinant containing both tag sequences was isolated by
394 crossing the recombinant OK26 to the previously described OK11 (57) and selecting

395 for plaques containing two fluorescent proteins by plaque assay. All viral recombinants
396 constructed for this paper are described in Table 1

397 **Fluorescent probes**

398 A set of 20 fluorescent probes was designed to correspond to each one of the two tag
399 sequences. The probes for the CMVp:mCherry and sequences SV40p:YPET were
400 conjugated on their 5' end to the fluorescent dyes cy3 and cy5 respectively. An
401 additional probe was designed to stain HSV1 viral DNA non-specifically. This probe
402 corresponds to the viral a' sequence and conjugated to the fluorescent dye Alexa Fluor
403 488 on its 5' end. Fluorescent probes were synthesized by Integrated DNA
404 Technologies (Coralville, IA, USA). The probes were dissolved in TE buffer to a stock
405 concentration of 10 μM. Probes from each set were pooled together in equal ratios
406 and kept in -20^{0}C before hybridization. Probes sequences are detailed in Table 2.

407 **Fluorescent in situ hybridization**

408 Cells where seeded and grown to confluence inside 12 well plates underlined with a
409 glass coverslip. Cells were infected at MOI 20 with 200 µl inoculums. The cells where
410 incubated on ice for 1 hour following the addition of the inoculums. The inoculums
411 were then removed and replaced with DMEM+10*FBS. The infected cells were
412 incubated on 37^{0}C for 6 hours. Cells where then fixed, permeabilized and hybridized
413 as in (58) with minor adjustments as follows: Denaturing of DNA was carried out in
414 95^{0}C instead of 75^{0}C for 2 minutes because of the relative high GC content of HSV1
415 DNA. Washing in SSCX0.1 was carried out in 63^{0}C instead of 60^{0}C. The fluorescent
416 probes were diluted into the hybridization mix to final concentration of 75 nM for each
417 probe set. Since the probes were directly labeled, all stages regarding antibody
418 staining and post-fixation were omitted from the protocol. Coverslips where then

419 mounted to glass slides using Fluoroshield mounting medium containing DAPI (Abcam,
420 Cambridge, MA, USA), sealed with nail polish and inspected under a confocal
421 microscope.

422 **Microscopy**

423 Viral plaques were visualized under a Nikon Eclipse Ti-E epifluorescence inverted
424 microscope. Single cell analysis by FISH assay was performed using a Nikon Eclipse
425 Ti microscope equipped with Yokogawa CSU X-1 spinning disc confocal system.

426 **Image analysis**

427 Nuclei segmentation: Nuclei were automatically segmented from the DAPI channel as
428 follows. Gaussian smoothing (σ = 2) was applied to the image followed by Otsu
429 thresholding (59) to partition the image to nuclei / background regions. The nuclei
430 segmentation was refined by morphological operators: opening (width = 3 pixels) to
431 exclude small excesses; closing and an additional opening (width = 20 pixels) to unify
432 regions that belong to the same nucleus; Filling holes; considering only connected
433 regions of area exceeding 900 pixels - the minimal nucleus size. The output of this
434 stage is a set of masks, each corresponds to a single nucleus.
435 RC segmentation: RCs were segmented from each fluorescent channel independently.
436 Three groups of intensities were observed within each nucleus: background - at
437 intensities close to those outside the nucleus; intermediate - above the background
438 levels; and bright - which are the replication centers. First, Gaussian smoothing was
439 applied (σ = 2) to the image. Second, background statistics were calculated (mean
440 intensity, standard deviation) from the pixels outside the nuclei masks. A threshold of
441 2.5 standard deviations above the background mean intensity level was calculated.
442 To exclude pixels with background intensities from further analysis, the threshold was

443 applied for each nucleus mask. Otsu thresholding was then applied to the remaining
444 pixels, pixels below the threshold were pooled and a new threshold of two standard
445 deviations above the mean was calculated. The pixels above these thresholds were
446 defined as the RCs. The segmentation refined by applying morphological operators:
447 opening - excluding small excess, closing - filling gaps, and opening again -
448 disconnecting independent replication centers; all with a square kernel of 3 pixels
449 width. Last, were holes filled to define the RCs. Parameters were optimized by visual
450 assessment of RC segmentation accuracy.
451 Manual selection of nuclei: Region for statistical analysis were manually selected
452 based on the accurate segmentation of RCs. Regions of accurate RC segmentation
453 were selected independently for each channel, the intersection (implying accurate
454 segmentation on both channels) was used for quantifications.
455 The program outputs required measurements such as nuclei area, number and area
456 of RCs in each channel of each nucleus and the size of overlapping area for each RC.
457 The data were then transferred into Microsoft excel for subsequent processing and
458 statistical analysis.
459 Code availability: The Matlab source code used for analysis is publically available at
460 https://github.com/assafzar/RecombinationHSV1.

461 **Acknowledgement**

462 We thank Eitan Erez Zahavi, Ariel Ionescu and Eran Perlson for advice and valuable
463 support and all Kobiler lab members for their comments.

464 **Funding**

465 This work was supported by grants from the Israel Science foundation (grant #1387/14)
466 to O.K., the EU CIG grant (FP7-2012-333653) to O.K., the National Institute of Health
467 (NS082240) to M.D.W., the United States - Israel Binational Science Foundation (grant

468 # 2015395) to O.K. and M.D.W., and a Marguerite Stolz Research Fellowship to O.K.
469 E.T. is supported by the Buchman Scholarship and A.Z. was supported by the National
470 Institute of Health Grant to Gaudenz Danuser (P01 GM103723). The funders had no
471 role in study design, data collection and analysis, decision to publish, or preparation
472 of the manuscript.

473

474 ## *References*

475 1. Kobiler O, Drayman N, Butin-Israeli V, Oppenheim A. 2012. Virus strategies for passing the
476 nuclear envelope barrier. Nucleus 3:526-39.
477 2. Burkham J, Coen DM, Weller SK. 1998. ND10 protein PML is recruited to herpes simplex virus
478 type 1 prereplicative sites and replication compartments in the presence of viral DNA
479 polymerase. J Virol 72:10100-7.
480 3. Dembowski JA, DeLuca NA. 2015. Selective recruitment of nuclear factors to productively
481 replicating herpes simplex virus genomes. PLoS Pathog 11:e1004939.
482 4. Lilley CE, Chaurushiya MS, Boutell C, Everett RD, Weitzman MD. 2011. The intrinsic antiviral
483 defense to incoming HSV-1 genomes includes specific DNA repair proteins and is
484 counteracted by the viral protein ICP0. PLoS Pathog 7:e1002084.
485 5. Liptak LM, Uprichard SL, Knipe DM. 1996. Functional order of assembly of herpes simplex
486 virus DNA replication proteins into prereplicative site structures. J Virol 70:1759-67.
487 6. Mohni KN, Livingston CM, Cortez D, Weller SK. 2010. ATR and ATRIP are recruited to herpes
488 simplex virus type 1 replication compartments even though ATR signaling is disabled. J Virol
489 84:12152-64.
490 7. Reyes ED, Kulej K, Pancholi NJ, Akhtar LN, Avgousti DC, Kim ET, Bricker DK, Spruce LA, Koniski
491 SA, Seeholzer SH, Isaacs SN, Garcia BA, Weitzman MD. 2017. Identifying Host Factors
492 Associated with DNA Replicated During Virus Infection. Mol Cell Proteomics 16:2079-2097.
493 8. Taylor TJ, Knipe DM. 2004. Proteomics of herpes simplex virus replication compartments:
494 association of cellular DNA replication, repair, recombination, and chromatin remodeling
495 proteins with ICP8. J Virol 78:5856-66.
496 9. Vogel JL, Kristie TM. 2013. The dynamics of HCF-1 modulation of herpes simplex virus
497 chromatin during initiation of infection. Viruses 5:1272-91.
498 10. Zhong L, Hayward GS. 1997. Assembly of complete, functionally active herpes simplex virus
499 DNA replication compartments and recruitment of associated viral and cellular proteins in
500 transient cotransfection assays. J Virol 71:3146-60.
501 11. Roizman B, Zhou G. 2015. The 3 facets of regulation of herpes simplex virus gene expression:
502 A critical inquiry. Virology 479-480:562-7.
503 12. Quinlan MP, Chen LB, Knipe DM. 1984. The intranuclear location of a herpes simplex virus
504 DNA-binding protein is determined by the status of viral DNA replication. Cell 36:857-68.
505 13. de Bruyn Kops A, Knipe DM. 1988. Formation of DNA replication structures in herpes virus-
506 infected cells requires a viral DNA binding protein. Cell 55:857-68.
507 14. Lukonis CJ, Weller SK. 1996. Characterization of nuclear structures in cells infected with
508 herpes simplex virus type 1 in the absence of viral DNA replication. J Virol 70:1751-8.

509 15. Taylor TJ, McNamee EE, Day C, Knipe DM. 2003. Herpes simplex virus replication
510 compartments can form by coalescence of smaller compartments. Virology 309:232-47.
511 16. Chang L, Godinez WJ, Kim IH, Tektonidis M, de Lanerolle P, Eils R, Rohr K, Knipe DM. 2011.
512 Herpesviral replication compartments move and coalesce at nuclear speckles to enhance
513 export of viral late mRNA. Proc Natl Acad Sci U S A 108:E136-44.
514 17. Sourvinos G, Everett RD. 2002. Visualization of parental HSV-1 genomes and replication
515 compartments in association with ND10 in live infected cells. EMBO J 21:4989-97.
516 18. Kobiler O, Brodersen P, Taylor MP, Ludmir EB, Enquist LW. 2011. Herpesvirus replication
517 compartments originate with single incoming viral genomes. MBio 2.
518 19. Sekine E, Schmidt N, Gaboriau D, O'Hare P. 2017. Spatiotemporal dynamics of HSV genome
519 nuclear entry and compaction state transitions using bioorthogonal chemistry and super-
520 resolution microscopy. PLoS Pathog 13:e1006721.
521 20. Muller HJ. 1964. The Relation of Recombination to Mutational Advance. Mutat Res 106:2-9.
522 21. Felsenstein J. 1974. The evolutionary advantage of recombination. Genetics 78:737-56.
523 22. Sanjuan R, Domingo-Calap P. 2016. Mechanisms of viral mutation. Cell Mol Life Sci 73:4433-
524 4448.
525 23. Holmes EC. 2008. Evolutionary history and phylogeography of human viruses. Annu Rev
526 Microbiol 62:307-28.
527 24. Renner DW, Szpara ML. 2017. The Impacts of Genome-wide Analyses on our Understanding
528 of Human Herpesvirus Diversity and Evolution. J Virol doi:10.1128/JVI.00908-17.
529 25. Brown SM, Ritchie DA, Subak-Sharpe JH. 1973. Genetic studies with herpes simplex virus
530 type 1. The isolation of temperature-sensitive mutants, their arrangement into
531 complementation groups and recombination analysis leading to a linkage map. J Gen Virol
532 18:329-46.
533 26. Honess RW, Buchan A, Halliburton IW, Watson DH. 1980. Recombination and linkage
534 between structural and regulatory genes of herpes simplex virus type 1: study of the
535 functional organization of the genome. J Virol 34:716-42.
536 27. Law GA, Herr AE, Cwick JP, Taylor MP. 2018. A New Approach to Assessing HSV-1
537 Recombination during Intercellular Spread. Viruses 10.
538 28. Lee K, Kolb AW, Sverchkov Y, Cuellar JA, Craven M, Brandt CR. 2015. Recombination Analysis
539 of Herpes Simplex Virus 1 Reveals a Bias toward GC Content and the Inverted Repeat
540 Regions. J Virol 89:7214-23.
541 29. Morse LS, Buchman TG, Roizman B, Schaffer PA. 1977. Anatomy of herpes simplex virus
542 DNA. IX. Apparent exclusion of some parental DNA arrangements in the generation of
543 intertypic (HSV-1 X HSV-2) recombinants. J Virol 24:231-48.
544 30. Schaffer PA, Aron GM, Biswal N, Benyesh-Melnick M. 1973. Temperature-sensitive mutants
545 of herpes simplex virus type 1: isolation, complementation and partial characterization.
546 Virology 52:57-71.
547 31. Tang KW, Norberg P, Holmudden M, Elias P, Liljeqvist JA. 2014. Rad51 and Rad52 are
548 involved in homologous recombination of replicating herpes simplex virus DNA. PLoS One
549 9:e111584.
550 32. Szpara ML, Gatherer D, Ochoa A, Greenbaum B, Dolan A, Bowden RJ, Enquist LW, Legendre
551 M, Davison AJ. 2014. Evolution and diversity in human herpes simplex virus genomes. J Virol
552 88:1209-27.
553 33. Kolb AW, Ane C, Brandt CR. 2013. Using HSV-1 genome phylogenetics to track past human
554 migrations. PLoS One 8:e76267.
555 34. Bowden R, Sakaoka H, Donnelly P, Ward R. 2004. High recombination rate in herpes simplex
556 virus type 1 natural populations suggests significant co-infection. Infect Genet Evol 4:115-23.
557 35. Reuven NB, Staire AE, Myers RS, Weller SK. 2003. The herpes simplex virus type 1 alkaline
558 nuclease and single-stranded DNA binding protein mediate strand exchange in vitro. J Virol
559 77:7425-33.

560 36. Schumacher AJ, Mohni KN, Kan YN, Hendrickson EA, Stark JM, Weller SK. 2012. The HSV-1
561 Exonuclease, UL12, Stimulates Recombination by a Single Strand Annealing Mechanism. Plos
562 Pathogens 8.
563 37. Weller SK, Coen DM. 2012. Herpes Simplex Viruses: Mechanisms of DNA Replication. Cold
564 Spring Harbor Perspectives in Biology 4.
565 38. Dasgupta UB, Summers WC. 1980. Genetic recombination of herpes simplex virus, the role
566 of the host cell and UV-irradiation of the virus. Mol Gen Genet 178:617-23.
567 39. Lilley CE, Carson CT, Muotri AR, Gage FH, Weitzman MD. 2005. DNA repair proteins affect
568 the lifecycle of herpes simplex virus 1. Proc Natl Acad Sci U S A 102:5844-9.
569 40. Wilkinson DE, Weller SK. 2006. Herpes simplex virus type I disrupts the ATR-dependent DNA-
570 damage response during lytic infection. J Cell Sci 119:2695-703.
571 41. Mohni KN, Dee AR, Smith S, Schumacher AJ, Weller SK. 2013. Efficient herpes simplex virus 1
572 replication requires cellular ATR pathway proteins. J Virol 87:531-42.
573 42. Edwards TG, Bloom DC, Fisher C. 2018. The ATM and Rad3-Related (ATR) Protein Kinase
574 Pathway Is Activated by Herpes Simplex Virus 1 and Required for Efficient Viral Replication. J
575 Virol 92.
576 43. Advani SJ, Weichselbaum RR, Roizman B. 2003. Herpes simplex virus 1 activates cdc2 to
577 recruit topoisomerase II alpha for post-DNA synthesis expression of late genes. Proc Natl
578 Acad Sci U S A 100:4825-30.
579 44. Smith S, Weller SK. 2015. HSV-I and the cellular DNA damage response. Future Virol 10:383-
580 397.
581 45. Shapira L, Ralph M, Tomer E, Cohen S, Kobiler O. 2016. Histone Deacetylase Inhibitors
582 Reduce the Number of Herpes Simplex Virus-1 Genomes Initiating Expression in Individual
583 Cells. Front Microbiol 7:1970.
584 46. Li Z, Fang C, Su Y, Liu H, Lang F, Li X, Chen G, Lu D, Zhou J. 2016. Visualizing the replicating
585 HSV-1 virus using STED super-resolution microscopy. Virol J 13:65.
586 47. Hayward GS, Jacob RJ, Wadsworth SC, Roizman B. 1975. Anatomy of herpes simplex virus
587 DNA: evidence for four populations of molecules that differ in the relative orientations of
588 their long and short components. Proc Natl Acad Sci U S A 72:4243-7.
589 48. Lee SW, Markham PF, Coppo MJ, Legione AR, Markham JF, Noormohammadi AH, Browning
590 GF, Ficorilli N, Hartley CA, Devlin JM. 2012. Attenuated vaccines can recombine to form
591 virulent field viruses. Science 337:188.
592 49. Mahiet C, Ergani A, Huot N, Alende N, Azough A, Salvaire F, Bensimon A, Conseiller E, Wain-
593 Hobson S, Labetoulle M, Barradeau S. 2012. Structural variability of the herpes simplex virus
594 1 genome in vitro and in vivo. J Virol 86:8592-601.
595 50. Rijsewijk FA, Verschuren SB, Madic J, Ruuls RC, Renaud P, van Oirschot JT. 1999.
596 Spontaneous BHV1 recombinants in which the gI/gE/US9 region is replaced by a
597 duplication/inversion of the US1.5/US2 region. Arch Virol 144:1527-37.
598 51. Cohen EM, Kobiler O. 2016. Gene Expression Correlates with the Number of Herpes Viral
599 Genomes Initiating Infection in Single Cells. PLoS Pathog 12:e1006082.
600 52. Drayman N, Karin O, Mayo A, Danon T, Shapira L, Rafael D, Zimmer A, Bren A, Kobiler O, Alon
601 U. 2017. Dynamic Proteomics of Herpes Simplex Virus Infection. MBio 8.
602 53. Alandijany T, Roberts APE, Conn KL, Loney C, McFarlane S, Orr A, Boutell C. 2018. Distinct
603 temporal roles for the promyelocytic leukaemia (PML) protein in the sequential regulation of
604 intracellular host immunity to HSV-1 infection. PLoS Pathog 14:e1006769.
605 54. Heaphy CM, de Wilde RF, Jiao Y, Klein AP, Edil BH, Shi C, Bettegowda C, Rodriguez FJ,
606 Eberhart CG, Hebbar S, Offerhaus GJ, McLendon R, Rasheed BA, He Y, Yan H, Bigner DD, Oba-
607 Shinjo SM, Marie SK, Riggins GJ, Kinzler KW, Vogelstein B, Hruban RH, Maitra A,
608 Papadopoulos N, Meeker AK. 2011. Altered telomeres in tumors with ATRX and DAXX
609 mutations. Science 333:425.

610 55. Hancock MH, Corcoran JA, Smiley JR. 2006. Herpes simplex virus regulatory proteins VP16
611 and ICP0 counteract an innate intranuclear barrier to viral gene expression. Virology
612 352:237-52.
613 56. Yao F, Schaffer PA. 1995. An activity specified by the osteosarcoma line U2OS can substitute
614 functionally for ICP0, a major regulatory protein of herpes simplex virus type 1. J Virol
615 69:6249-58.
616 57. Taylor MP, Kobiler O, Enquist LW. 2012. Alphaherpesvirus axon-to-cell spread involves
617 limited virion transmission. Proc Natl Acad Sci U S A 109:17046-51.
618 58. Cremer M, Grasser F, Lanctot C, Muller S, Neusser M, Zinner R, Solovei I, Cremer T. 2008.
619 Multicolor 3D fluorescence in situ hybridization for imaging interphase chromosomes.
620 Methods Mol Biol 463:205-39.
621 59. Otsu N. 1979. Threshold Selection Method from Gray-Level Histograms. Ieee Transactions on
622 Systems Man and Cybernetics 9:62-66.

623

624

625

626 **Figure 1. Schematic representation of dual colour FISH assay**. (**A)** A series of viral
627 recombinants with two unique tag sequences (designated red and green) inserted into various
628 loci of the parental genome. Illustration of the insertion sequences (colour boxes) and viral
629 genomes (black line with repeats marked in gray boxes). Illustrations are not to scale. (**B)** Two
630 sets of probes conjugated to distinct fluorophores, each set corresponds to one tag sequence.
631 (**C)** Illustration of expected results, in which the gray nucleus contains viral RCs originating
632 from genomes with one tag sequences (either red or green), two tag sequences (yellow) or
633 no tag sequence (black). The expected results in case of infection with tag sequences on the
634 same locus of two co-infecting genomes **(I)**, with tag sequences on separate loci in two co-
635 infected genomes where recombination takes place before DNA replication **(II)** or following
636 DNA replication **(III)** and with two tag sequences in the same genome **(IV)**. **(D)** Representative
637 images of viral plaques initiating from progeny viruses collected from Vero cells co-infected
638 with different viral recombinants as marked above each image. Scale bar is 100 μm.

639 **Figure 2. Observed patterns of RC interactions. (A-D)** Representative images of Vero cells
640 infected with viral isolates containing two genomic tags, each corresponding to a set of
641 fluorescent probes. The probe sets are imaged separately in red and green (I and II) and
642 merged (III). Four observed patterns of interaction between RCs are represented: **(A)** RCs
643 containing different tag sequences come into contact without overlap (orange arrowhead),
644 imaged from cells infected by two viral recombinants containing tag sequences on the same
645 genomic locus (OK25 and OK35). **(B)** RCs containing different tag sequences overlap at their
646 periphery (white arrowhead), imaged from cells infected with two viral recombinants containing
647 tag sequences on separate genomic loci (OK32 and OK35). **(C)** RC containing one tag
648 sequence overlap completely within a larger RC with the second tag (black arrowhead) imaged
649 from cells infected with two viral recombinants containing tag sequences on separate genomic
650 loci (OK26 and OK35). **(D)** Entirely overlapping RCs, imaged from cells infected by a viral
651 recombinant containing two tag sequences on the same genome in separate loci (OK31).
652 DAPI nuclear stain is presented in gray. Scale bar is 5μm. **(E)** Percent of each of the observed
653 RCs interactions (A to D) out of total RCs interactions. Manually counted at the different co-
654 infection conditions. >60 cells and >100 RCs interactions per infection type were counted.

655 **Figure 3. Patterns of RC interactions on U2OS cells. (A-C)** Representative images of
656 U2OS cells infected with either **(A)** OK25 and OK35, **(B)** OK32 and OK35 or **(C)** OK31 viral
657 recombinants. The probe sets are imaged separately in red and green (I and II) and merged
658 (III). Arrowheads are colour coded as in figure 2. DAPI is presented in gray. Scale bar is 5μm.
659 (**D**) Percent of each of the observed RCs interactions out of total RCs interactions. Manually
660 counted at the different co-infection conditions. >50 cells and >100 RCs interactions per
661 infection type were counted.

662 **Figure 4. HR enhances overlap between viral genomes.** Vero cells **(A, C, E)** and U2OS
663 cells **(B, D, F)** were infected with the viral isolates OK35 & OK25 where tags are inserted into
664 the same genomic locus (blue), the viral isolates OK35 & OK32 (yellow) or OK35 & OK26
665 (orange) containing tags on separate genomic loci and the viral isolate OK31 containing two
666 tag sequences on a single viral genome (gray). **(A and B)** Each column represents the
667 percentage of cells showing no overlap out of the total number of cell analysed for each
668 infection condition. *P < 0.05, ***P < 0.001; by Z.score proportion test. **(C and D)** Each column
669 represents the average relative overlapping area calculated from all cells (with detectable
670 overlap) infected under the same condition. Error bars represent standard error of the means.
671 *P < 0.05, ** P < 0.01; ***P < 0.001; by t test. **(E and F)** Individual cells were plotted to compare
672 the relative overlapping area to the nuclear area. All analyses were conducted on images
673 generated from three independent experimental repeats done on different days with viral
674 stocks prepared and tittered separately.

675 **Figure 5. Nuclear size correlates with the number of RCs per cell.** Cells where co-infected
676 with the viral recombinants OK35 & OK25 (blue), OK35 & OK32 (yellow) and OK35 & OK26
677 (orange). Comparing the mean number of RCs per cell **(A)** and the mean nuclear area **(B)**
678 between Vero (bright coloured columns) and U2OS (dark coloured columns). Error bars
679 represent standard error of the means. **(C-H)** Individual Vero **(C, E, G)** and U2OS **(D, F, H)**
680 cells were plotted to compare the number of RCs per cells **(C, D)**, the total area of RCs per
681 cell **(E, F)** and the average area of each RCs **(G, H)** to the nuclear area. A trend line (colour
682 coded as above) was calculated using the ordinary least squares (OLS) method is presented
683 for each infection condition. All analyses were conducted on images generated from three
684 independent experimental repeats done on different days with viral stocks prepared and
685 tittered separately.

686 **Figure 6. Replication compartments contain at least one tag sequence.** Representative
687 images of U2OS cells infected with two viral isolates containing tag sequences at different
688 genomic loci (OK35 and OK32). The cells were hybridized with two probes conjugated to three
689 distinct fluorophores. I. Detection of the OK35 tag sequence is shown in red. II. Detection of
690 the OK32 tag sequence is shown in green. III. Detection of the viral 'a' sequence (detect HSV
691 DNA non-specifically) is shown in blue. Overlays of two and three colours are shown in panels
692 IV and V, respectively. DAPI is presented in gray. Scale bar is 5 µm.

693

694

Viral recombinant	Tag sequence	Locus of insertion	Insertion start point
OK25	SV40p:YPET	Between the ORFs UL3 and UL4	11736
OK26	SV40p:YPET	Between the ORFs UL55 and UL56	116153
OK32	SV40p:YPET	Between the ORFs UL37 and UL38	84252
OK31	SV40p:YPET CMVp:mCherry	Between the ORFs UL55 and UL56 Between the ORFs UL37 and UL38	116153 84252
OK35	CMVp:mCherry	Between the ORFs UL37 and UL38	11736

695 **Table 1. List of viral recombinants used in this work**

696

697

SV40p:YPET	CMVp:mCherry	HSV-1 a' sequence
CTTGCATCTCAATTAGTCAGCAACC	CTTAAGCCCATATATGGAGTTCCGC	CCCCCCGCTCCTCCCCCCGCT
GCTACGGCGTGCAGTGCTTCGCCAG	TAACTTACGGTAAATGGCCCGCCTG	
TCCGCCCATTCTCCGCCCCATCGCT	AACGACCCCCGCCCATTGACGTCAA	
ATTTATGCAGAGGCCGAGGCCGCCT	GACGTATGTTCCCATAGTAACGCCA	
CCTCTGAGCTATTCCAGAAGTAGTGAGG	GACTTTCCATTGACGTCAATGGGTG	
GGAGGCCTAGGCTTTTGCAAAAAGC	CGGTAAACTGCCCACTTGGCAGTAC	
GACACAACAGTCTCGAATTTAAGGCTAG	ATGGGCGTGGATAGCGGTTTGACTC	
CTGTTCACCGGAGTGGTGCCTATCC	CCAAAATGTCGTAACAACTCCGCCC	
CGACGCTACCTACGGAAAGCTGACC	ATGGGCGGTAGGCGTGTACGGTGGG	
GTGCCTTGGCCCACCCTTGTGACCA	GCAGAGCTGGTTTAGTGAACCGTCA	
ACCACATGAAGCAGCACGACTTCTT	GATAACATGGCCATCATCAAGGAGT	
AACATCCTGGGCCACAAGCTGGAGT	GTGGATAGCGGTTTGACTCACGGG	
CATCACCGCCGACAAGCAGAAGAAC	GTCCCCTCAGTTCATGTACGGCTCC	
CCCATCGGCGACGGTCCCGTGCTGC	GTGGTGACCGTGACCCAGGACTCCT	
CCTGACAACCACTACCTGAGCTACCAG	GGACGGCGAGTTCATCTACAAGGTG	
TTCAAGGACCCCAACGAGAAGCGGG	CCCGTAATGCAGAAGAAGACCATGG	
CACGACTGTGCCTTCTAGTTGCCAG	CTCCGAGCGGATGTACCCCGAGGAC	
GACCCTGGAAGGTGCCACTCCCACT	CGGCGCCTACAACGTCAACATCAAG	
GGAAATTGCATCGCATTGTCTGAGT	GTCTCCACCCCATTGACGTCAATGG	
GGAAGACAATAGCAGGCATGCTGGG	CATCGCTATTACCATGGTGATGCGG	

698 **Table 2. List of fluorescently labelled probes for FISH.**

699

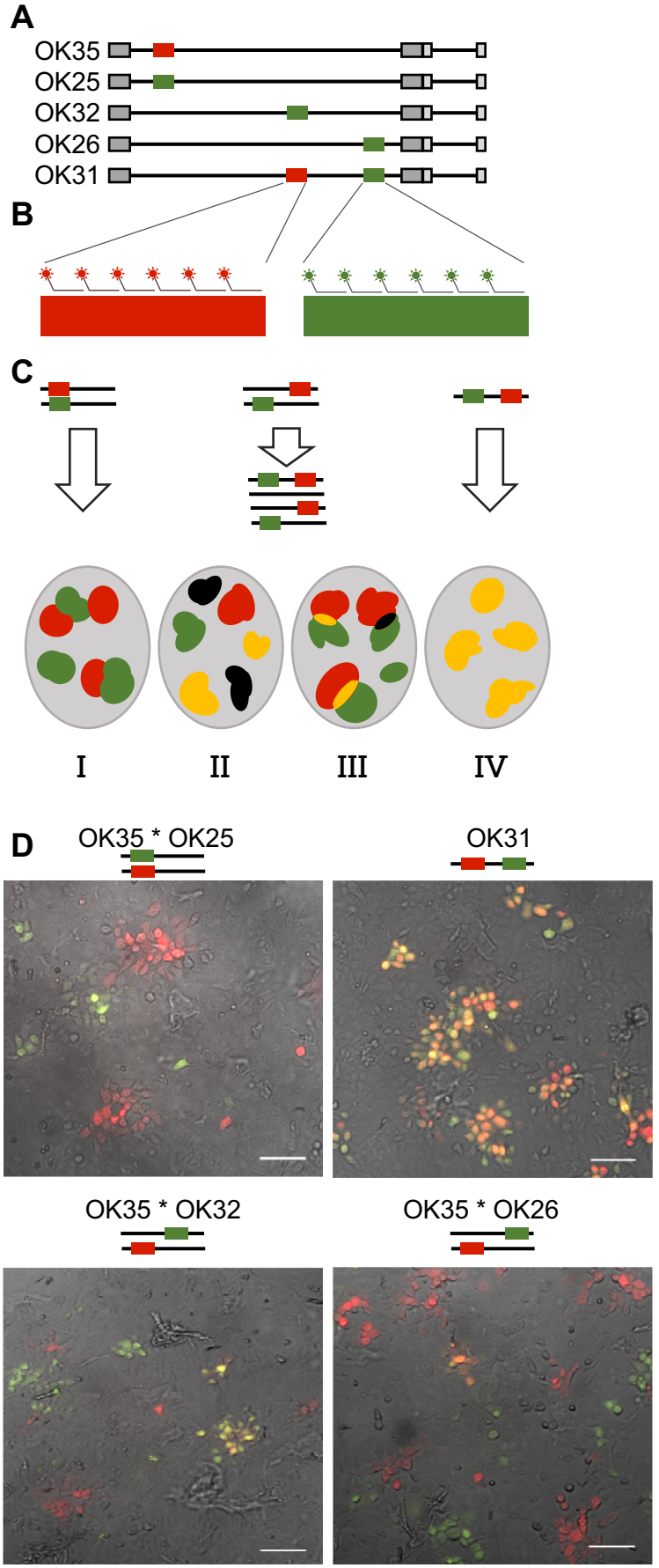
A
OK35
OK25
OK32
OK26
OK31
B
C
I
II
III
IV
D
OK35 * OK25
OK31
OK35 * OK32
OK35 * OK26

Figure 1

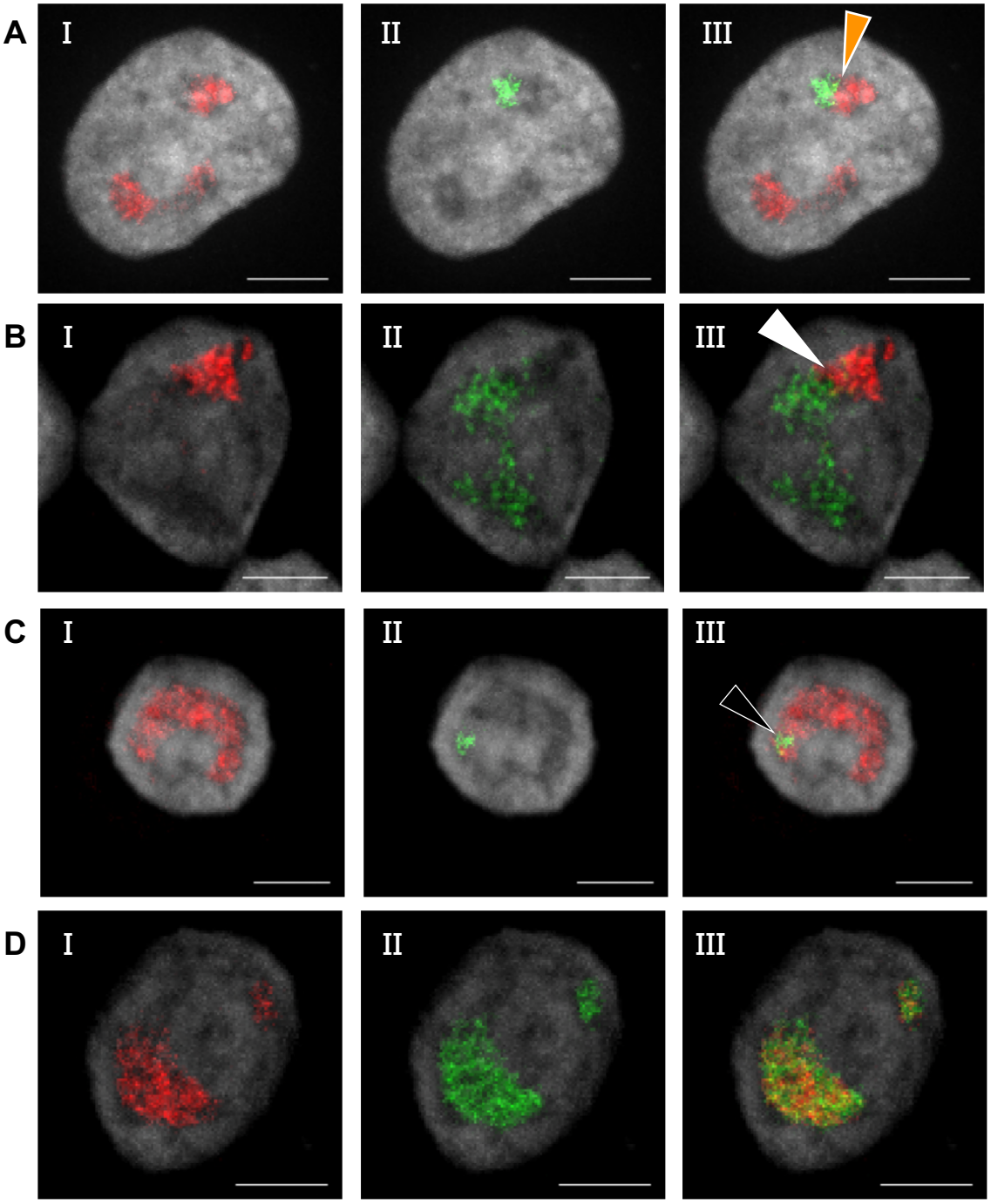

E

	A – minimal overlap	B - periphery overlap	C- Full overlap within larger RC	D – Full overlap
OK25*OK35	33.0	60.4	6.6	0
OK32*OK35	28.7	50.4	15.7	5.2
OK26*OK35	18.4	71.1	8.8	1.8
OK31	0	6.4	5.7	87.9

Figure 2

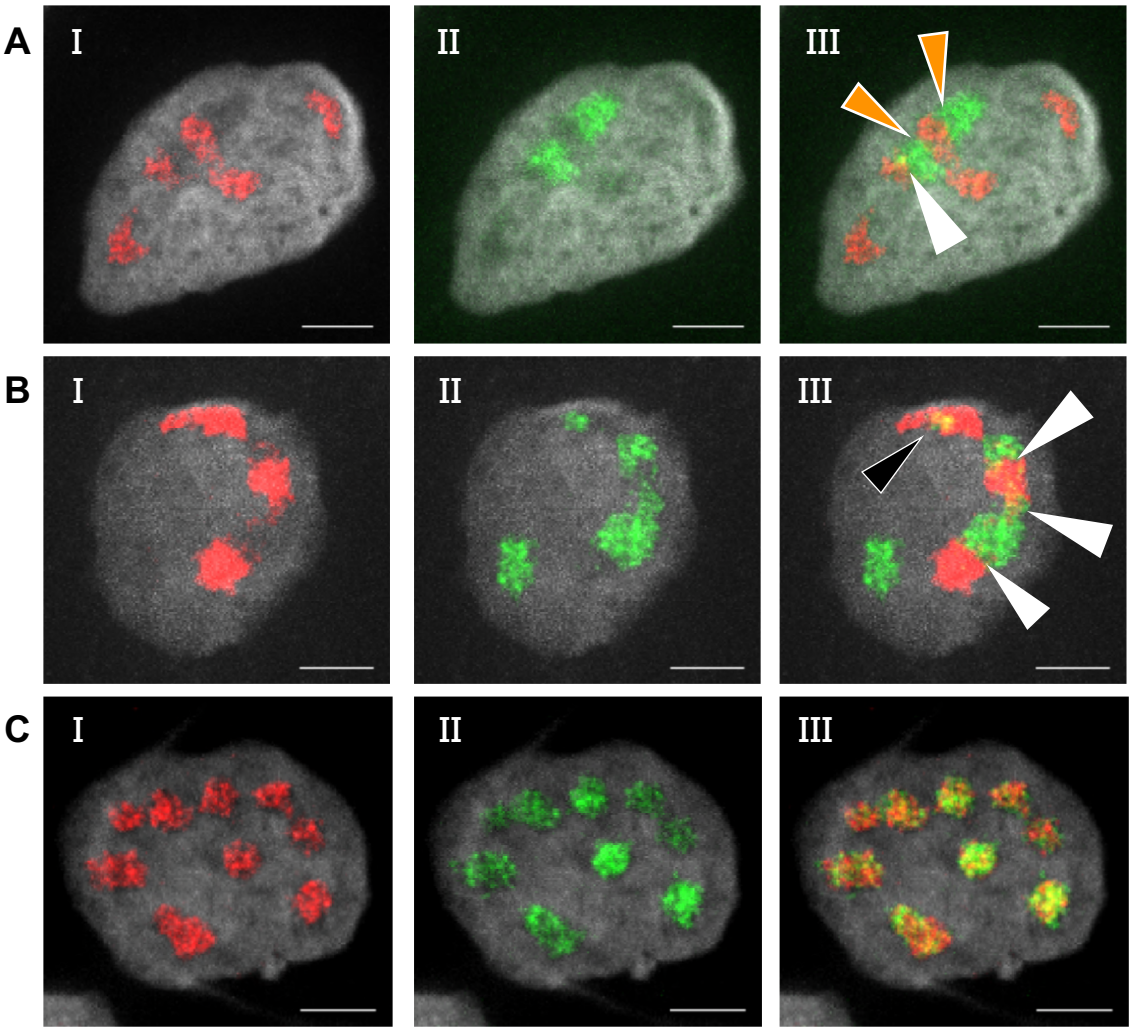

D

	A – minimal overlap	B - periphery overlap	C- Full overlap within larger RC	D – Full overlap
OK25*OK35	36.0	59.6	4.4	0
OK32*OK35	16.5	73.3	9.7	0.6
OK26*OK35	23.5	69.9	4.6	2.0
OK31	0.6	8.0	4.0	87.4

Figure 3

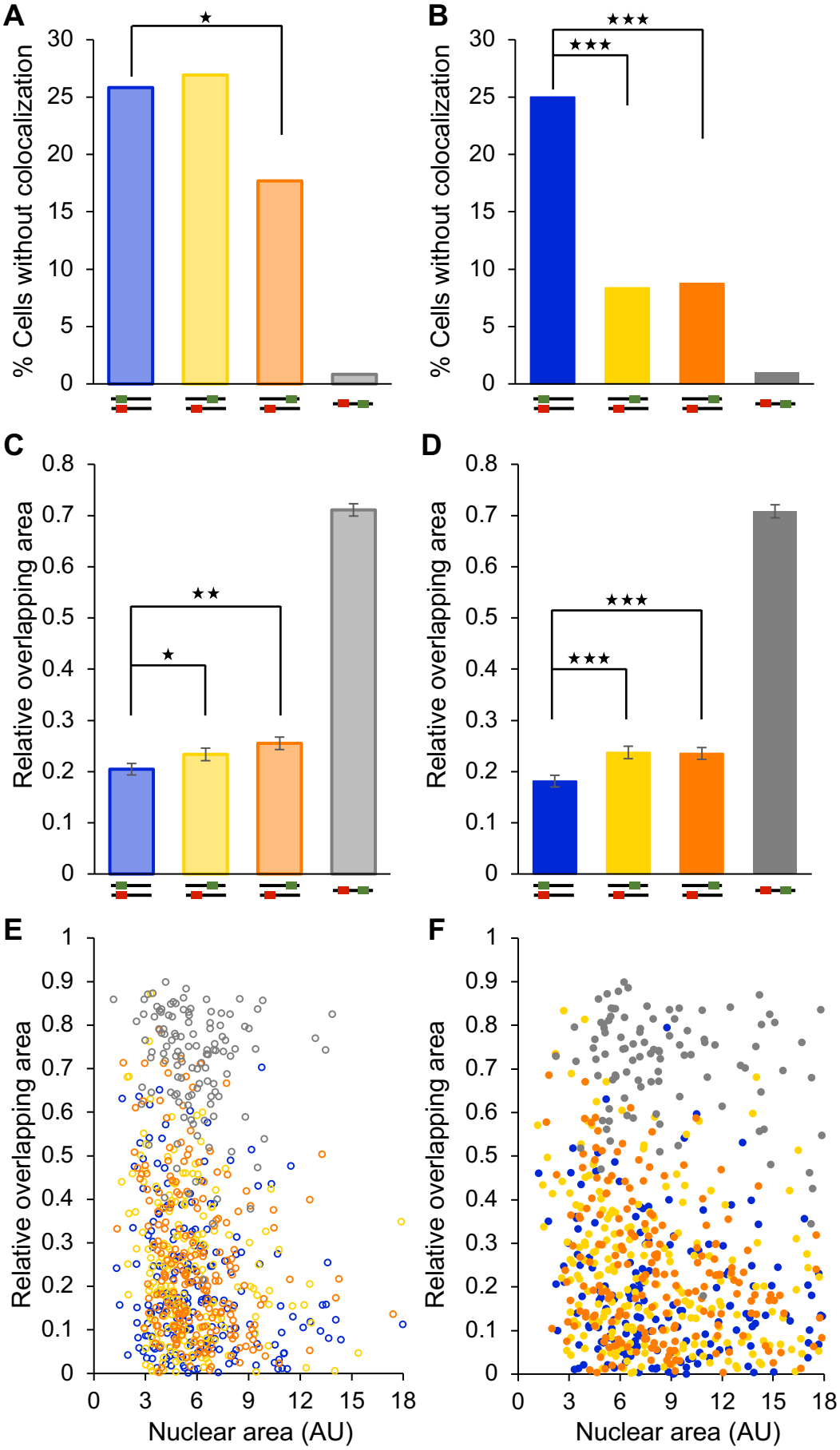
A
B
C
D
E
F
% Cells without colocalization
Relative overlapping area
Nuclear area (AU)
0
5
10
15
20
25
30
0.1
0.2
0.3
0.4
0.5
0.6
0.7
0.8
0.9
1
3
6
9
12
15
18

Figure 4

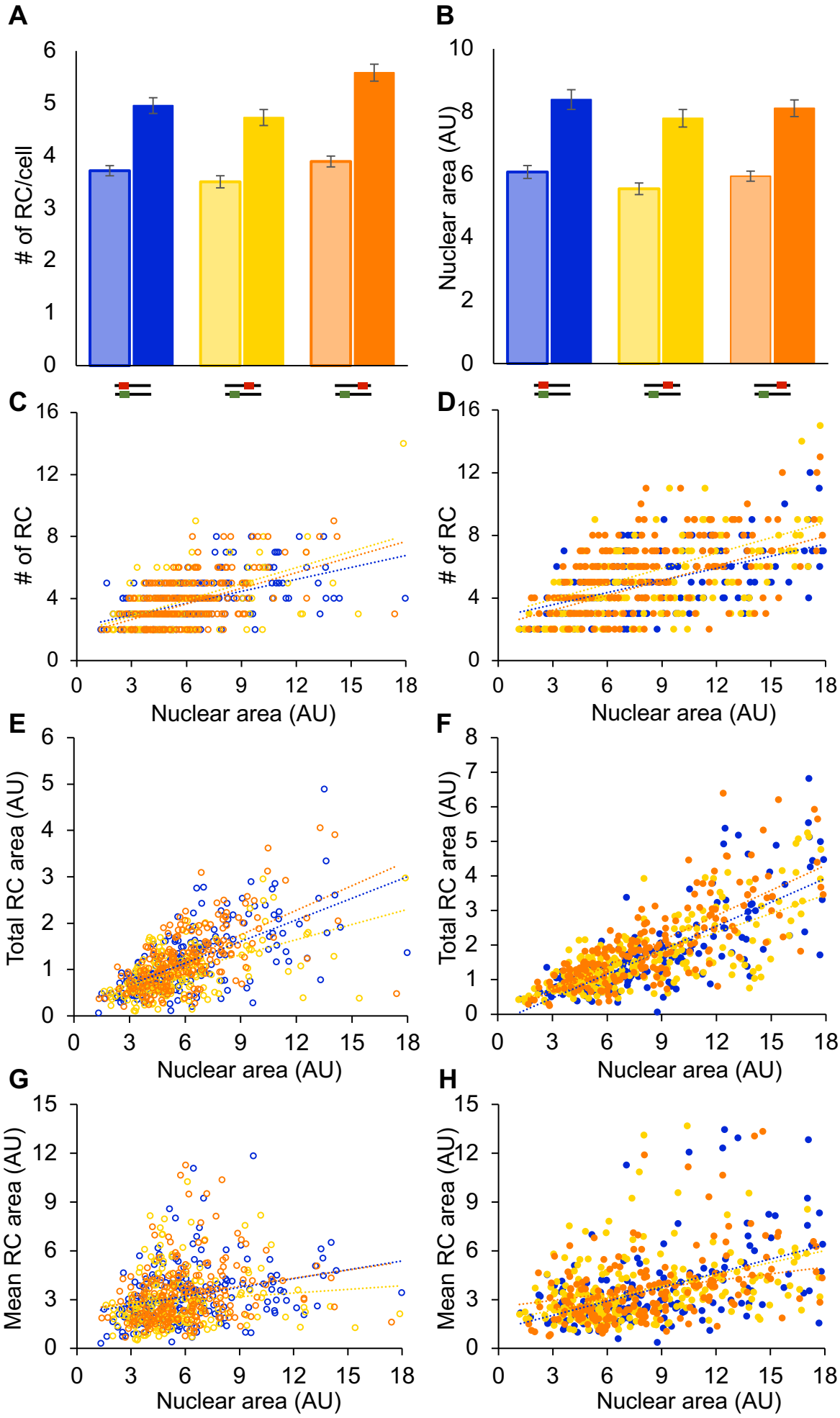
A
# of RC/cell
B
Nuclear area (AU)
C
# of RC
Nuclear area (AU)
D
# of RC
Nuclear area (AU)
E
Total RC area (AU)
Nuclear area (AU)
F
Total RC area (AU)
Nuclear area (AU)
G
Mean RC area (AU)
Nuclear area (AU)
H
Mean RC area (AU)
Nuclear area (AU)

Figure 5

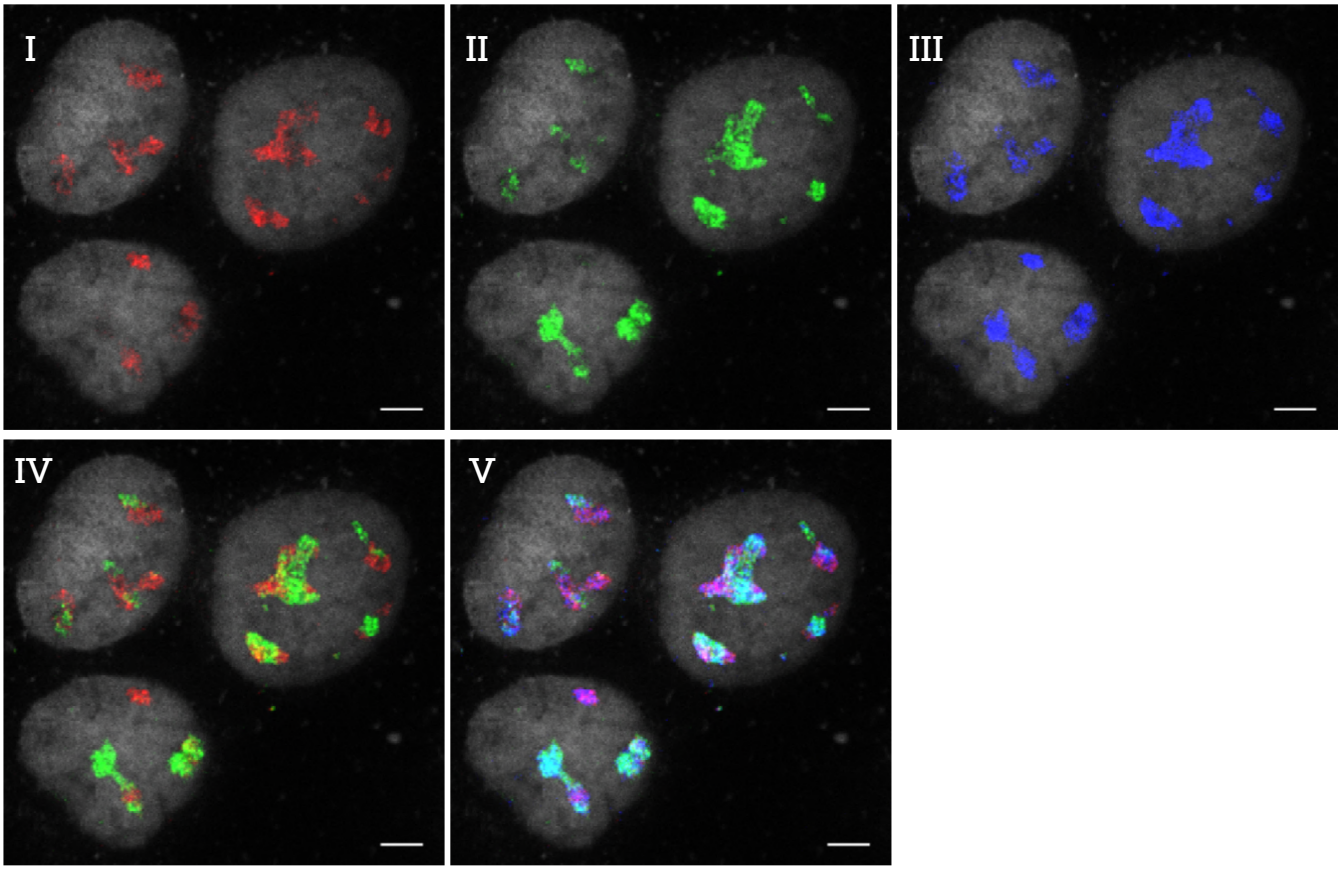

Figure 6